

# Modeling the Behavior of Confined Colloidal Particles Under Shear Flow

F.E. Mackay,<sup>a</sup> K. Pastor,<sup>a</sup> M. Karttunen,<sup>b</sup> and C. Denniston<sup>a</sup>

Received Xth XXXXXXXXXX 20XX, Accepted Xth XXXXXXXXXX 20XX

First published on the web Xth XXXXXXXXXX 200X

DOI: 10.1039/b000000x

We investigate the behavior of colloidal suspensions with different volume fractions confined between parallel walls under a range of steady shears. We model the particles using molecular dynamics (MD) with full hydrodynamic interactions implemented through the use of a lattice-Boltzmann (LB) fluid. A quasi-2d ordering occurs in systems characterized by a coexistence of coupled layers with different densities, order, and granular temperature. We present a phase diagram in terms of shear and volume fraction for each layer, and demonstrate that particle exchange between layers is required for entering the disordered phase.

## 1 Introduction

Confined particle suspensions are found in a range of applications including surface coatings and lubricants. A thorough understanding of their rheological properties is important as the functionality of these products is highly dependent on their response to shear. In a bulk system, the magnitude of the applied shear dictates the resulting steady state behavior. For shear rates above a critical value, any underlying order is destroyed, and a melted steady state configuration arises.<sup>1–3</sup> In contrast, at lower shear rates a reentrant ordering may occur in which particles rearrange themselves into hexagonally ordered layers aligned along the flow.<sup>4–8</sup> Such shear alignment can be used as a mechanism for manufacturing colloidal crystals with minimal imperfections, desirable for photonic band gap materials,<sup>9,10</sup> since shear can both speed up the crystallization process as well as greatly improve the quality of the growing crystal.<sup>11</sup> In the presence of confining geometries, a higher degree of ordering tends to form near the walls compared with the sample center,<sup>6,7</sup> while packing constraints may lead to the formation of new structures not observed in bulk.<sup>12,13</sup> When shear is applied to colloidal glasses, the resulting behavior provides insight into the flow properties of yield stress materials.<sup>14,15</sup>

The mechanisms responsible for shear induced structural transitions are not fully understood. Compared with a quiescent sample, both melting and crystallization under shear appear to proceed quite differently.<sup>16</sup> Based on confocal mi-

croscopy, Wu et al.<sup>17</sup> observed that shear induced crystallization advances through a collective reordering of the sample, while they suggest that the melting process, which is accompanied by large fluctuations in crystalline order, involves the nucleation of local domains alternating between disordered and ordered states. Brownian dynamics simulations of a pair of layers driven past one another also hint at this latter behavior, with the layers undergoing cycles of order and disorder.<sup>18</sup> However, these simulations ignored hydrodynamics and did not allow for particle exchange between the layers, which may be important for the melting process. For instance, Palberg et al.<sup>19</sup> noted that the systems they observed first melted in the layer-perpendicular direction and with a different mechanism than in-plane melting, although they did not study this behavior in detail. In addition, hydrodynamic interactions can play an important role in the resulting behavior. For example, at lower volume fractions than those considered here, a balance between hydrodynamic and interparticle interactions leads to the formation of log-rolling particle strings normal to the plane of shear.<sup>20,21</sup>

To gain further insight into shear induced melting and crystallization, we performed hybrid LB-MD simulations of highly confined colloidal systems subject to shear. In contrast to the majority of previous simulations which tend to focus exclusively on the colloidal particles, either by not including the effects of hydrodynamic interactions<sup>22,23</sup> or employing techniques such as the force coupling method,<sup>7</sup> which do not directly yield fluid data, our simulations not only track the individual particle motions but also produce fluid flow data on the entire simulation domain.

<sup>a</sup> Department of Applied Mathematics, The University of Western Ontario, London, Ontario N6A 5B8, Canada; E-mail: fmackay2@uwo.ca, cdeniston@uwo.ca

<sup>b</sup> Department of Chemistry & Waterloo Institute for Nanotechnology, University of Waterloo, Waterloo, Ontario N2L 3G1, Canada; E-mail: mkarttu@gmail.com

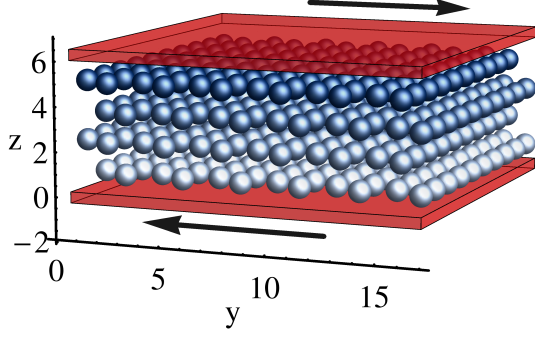


**Fig. 1** Initial system, composed of four layers each of 120 particles, arranged in a hexagonal array. Particle size has been reduced for visualization; a range of particle sizes was used. Moving walls are present at  $z = 0$ , and  $z = 5.88\mu m$ .

## 2 Simulation Details

Our systems contained 480 colloidal particles confined in a region of  $16.56 \times 16.56 \times 5.88 \mu m$ . Parallel walls were present in the  $z$ -direction, confining the particles into 4 layers. Periodic boundary conditions were applied in  $x$ - and  $y$ -directions. Larger 8 layer systems were simulated producing results similar to the 4 layer case. Hence, for efficiency, we focussed on the 4 layer systems. Figure 1 shows the initial configuration. For simplicity, we considered a fluid with viscosity and density corresponding to water. Shear was established by moving the upper and lower walls at constant, opposite velocities,  $\pm v_y \hat{y}$ . Particle radii and wall velocities were varied to investigate a range of shear rates and colloidal volume fractions.

Simulations were performed using LAMMPS<sup>24</sup> along with a lattice-Boltzmann fluid package.<sup>25</sup> The latter uses a discretized version of the Boltzmann equation to solve for the fluid motion governed by the Navier-Stokes equations,

$$\begin{aligned} \partial_t \rho + \partial_\beta (\rho u_\beta) &= 0 \\ \partial_t (\rho u_\beta) + \partial_\beta (\rho u_\alpha u_\beta) &= -\partial_\alpha P_0 + F_\alpha + \\ &\quad \eta \partial_\beta (\partial_\alpha u_\beta + \partial_\beta u_\alpha), \end{aligned} \quad (1)$$

on a uniform grid. Here,  $\rho$  is the fluid density,  $\mathbf{u}$  is the local fluid velocity,  $P_0$  is the pressure set to  $\rho/3(\Delta x^2/\Delta t^2)$ ,  $\mathbf{F}$  is a local, external force resulting from the presence of the colloidal particles, and  $\eta$  is the shear viscosity. For all simulations, we used  $\Delta x = 0.06 \mu m$  for the LB grid spacing, and a timestep of  $\Delta t = 0.0006 \mu s$ .

Each of the colloidal particles was represented by a spherical shell of 3612 evenly distributed MD particles, referred to as nodes. This enables the colloidal particles to be modeled off lattice, using molecular dynamics techniques. Here, we made use of the rigid fix in LAMMPS, constraining each set of nodes to move and rotate together as a single rigid body. Coupling between the colloidal particles and the fluid is then

accomplished through the use of conservative forces applied locally to both the particle nodes and the fluid according to

$$F = \pm \gamma (\mathbf{v} - \mathbf{u}), \quad (2)$$

where the  $+$  sign corresponds to the force of the node on the fluid, and the  $-$  sign corresponds to the force of the fluid on the node. Here,  $\mathbf{v}$  is the velocity of the node,  $\mathbf{u}$  is the local fluid velocity, and  $\gamma$  is given by

$$\gamma = \frac{2m_u m_v}{m_u + m_v} \frac{1}{\Delta t_{collision}}, \quad (3)$$

where  $m_v$  is the mass of the node,  $m_u$  is the mass of the fluid, and the collision time,  $\Delta t_{collision}$ , is set equal to the relaxation time in the lattice-Boltzmann fluid. These forces were calculated from the impulses that would arise during an elastic collision between the MD nodes and a mass of fluid at the node location. Full details, along with numerous tests of this method can be found in Mackay et. al.<sup>25,26</sup>

In addition to the hydrodynamic forces, we implemented interactions between the colloids by assigning an additional MD particle to each colloidal center interacting via the truncated & shifted Lennard-Jones potential

$$V(r) = \begin{cases} 4\epsilon \left[ \left( \frac{\sigma}{r} \right)^{12} - \left( \frac{\sigma}{r} \right)^6 \right] - \epsilon, & \text{if } r \leq r_c \\ 0, & \text{if } r > r_c, \end{cases} \quad (4)$$

where  $\sigma = r_c/2^{1/6}$ . These interactions are important to prevent particle overlap. We chose  $\epsilon = 10$  and set the cutoff distance to  $r_c = 2(a + \Delta x)$ , where  $a$  is the MD node placement radius, in order to prevent both an overlap of the MD nodes and their associated LB grid representations. A similar interaction was also implemented between the central MD nodes and the walls at  $z = 0$ , and  $z = 5.88\mu m$ . For this interaction we set  $\epsilon = 20$ , and  $r_c = a + 3\Delta x$  ensuring that no particles left the simulation domain.

Since the resulting colloidal behavior can be quite disordered at times, we make use of the colloidal granular temperature<sup>27</sup>,  $T$ , in order to characterize the colloidal fluctuations. For a given layer of particles in the system, this temperature is calculated according to

$$T = \frac{1}{3} \left( \langle (v_x - \bar{v}_x)^2 \rangle + \langle (v_y - \bar{v}_y)^2 \rangle + \langle (v_z - \bar{v}_z)^2 \rangle \right), \quad (5)$$

where  $\bar{v}_i$  is the average velocity of the colloidal particles in the layer, and the angular brackets correspond to an average over all particles in the layer. A similar calculation is also performed for the fluid, proportional to the kinetic energy per unit mass associated with velocity deviations in the fluid.

## 3 Results

Simulations were performed for three different particle radii, corresponding to total volume fractions of 0.521, 0.588, and

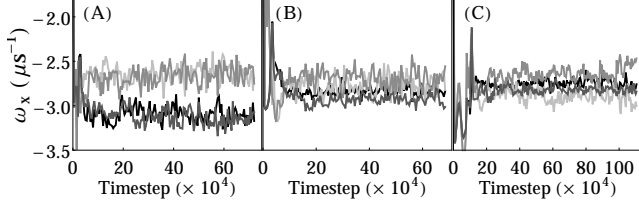


**Fig. 2** Average angular velocity in each particle layer as a function of time for systems with a shear rate of  $6.8 \mu s^{-1}$  and volume fractions of (A) 0.521, (B) 0.588 and (C) 0.645. Darker grey: particle layers near the walls. Lighter grey: middle layers.

0.645, along with shear rates of 1.7, 3.4, 5.1 and  $6.8 \mu s^{-1} \hat{y}$ . We chose these high shear rates in order to focus on the effects of hydrodynamic interactions; the shear in our systems results in colloidal granular temperatures much greater than  $k_B T$ , isolating the hydrodynamic effects from those due to thermal fluctuations. This shear results in the particles rotating along the  $x$ -direction, as illustrated in Figure 2. However, depending on the shear rate and volume fraction in the system, not all particle layers rotate with the same average rate. This can be seen in Figure 2 (A) where the two (disordered) middle layers exhibit a smaller average angular velocity than the outer layers.

The initial configuration chosen does not favour shear along the  $y$ -direction; while shear along  $x$  would simply allow the hexagonal layers to slide over one another, shear directed along  $y$  requires particles in adjacent layers to “hop” over one another. Therefore, this initial particle arrangement is not stable against shear and the systems evolve into a variety of different configurations depending on the volume fraction and shear rate.

For the majority of systems considered, we observed a migration of particles from the middle layers towards the walls, consistent with previous works.<sup>7</sup> This leads to a range of different layer volume fractions. We therefore focus on the per layer behavior of our systems by dividing the system along the vertical direction into distinct regions of equal size, and assigning particles to each of these layers based on the location of their center of mass. We then quantify the behavior in each layer through the local 2D orientational order parameter

$$\psi_6(r_{jk}) = \frac{1}{n} \sum_{k=1}^n e^{i6\theta(r_{jk})}, \quad (6)$$

averaged over all the particles in each layer. Here,  $n$  corresponds to the number of nearest neighbours of particle  $j$ , calculated as the particles,  $k$ , in the same layer as  $j$ , with a surface to surface separation from  $j$  within a particle diameter, and  $\theta(r_{jk})$  is the angle between the vector connecting particle  $j$  with its neighbour  $k$  and an arbitrary fixed axis. For a perfectly ordered hexagonal system,  $\langle |\psi_6| \rangle = 1$ .

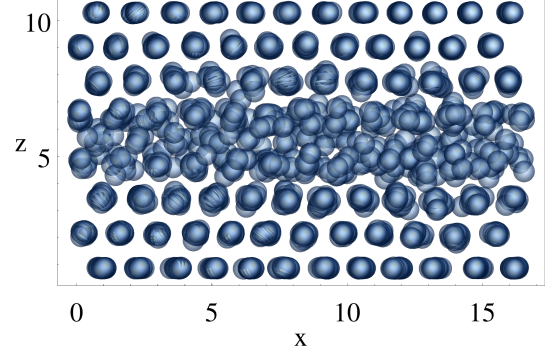


**Fig. 3** Snapshot in the  $x$ - $z$  plane of an initially ordered eight layer system which has phase separated into six ordered outer layers, and two disordered middle layers. Note that the size of the colloidal particles has been reduced here for clarity.

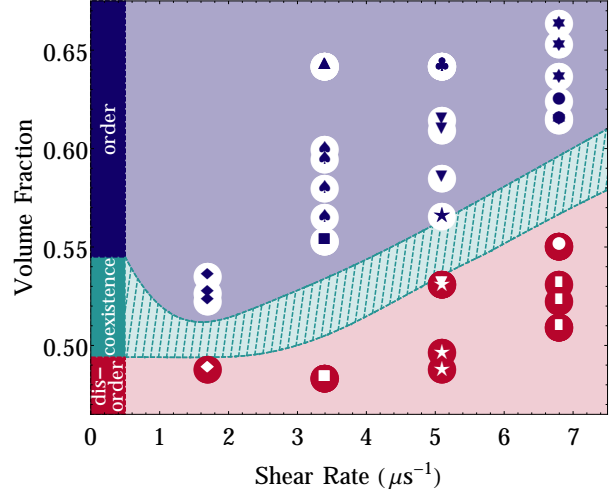
Simulations were run until steady state was achieved and the order parameter amplitude in each layer was observed to fluctuate around a constant value. The layers of the resulting systems are characterized as disordered when  $\langle |\psi_6| \rangle < 0.6$ , or hexagonally ordered with alignment now along the flow direction when  $\langle |\psi_6| \rangle > 0.6$ . For high volume fractions with low to moderate shear rates, all layers reorder to form hexagonal particle arrangements aligned along the flow. In contrast, at low volume fractions and high shear, the steady state configuration consists of four disordered layers. For the remaining systems, a phase separation occurs, leading to the appearance of distinct ordered and disordered layers. The formation of distinct layers as opposed to regions of order and disorder within a given layer could be a finite size effect. However, this behavior is consistent with experiments in which hexagonal layers are observed coexisting with a fluid phase.<sup>17,19,28</sup> Similar behavior was also observed in an eight layer system (size  $16.56 \times 33.12 \times 11.16 \mu m$ ), where the system phase separated into six ordered and two disordered layers as shown in Figure 3.

Figure 4 presents our results in the form of a per layer phase diagram, illustrating the layer order as a function of volume fraction and applied shear rate. As expected, *high shear rates* tend to induce disorder, raising the colloidal melting volume fraction above that of a system in the absence of shear. Shear alignment acts at *lower shear rates*, enabling ordered layers to form at volume fractions reduced from the stationary system value. (At even lower shear rates, we expect the melting & freezing volume fractions to return to their zero shear levels; due to the significantly longer simulation times we have omitted these from our analysis.) As Fig. 4 shows, the location of the order-disorder phase boundary is mapped out by the systems which experience *phase separation*. In these systems, higher volume fraction ordered outer layers coexist with lower

volume fraction disordered middle layers, where the number of each type that develop depends on both the location of the phase boundary and the size of the associated coexistence region, inaccessible to a pure (ordered or disordered) phase. For example, consider the system shown in the lower left hand corner of Fig. 4 consisting of three ordered layers and one disordered middle layer. The asymmetry of the system clearly points to an inaccessible region on the phase diagram separating the ordered and disordered phases, explaining why the two middle layers do not form the same phase with volume fractions which would then be located inside this region. The ability of these systems to phase separate is enabled only through a migration of particles towards the walls, coupled with lower granular temperature,  $T$ , near the walls (see Fig. 5). These lower observed temperatures arise from a reduction in the degrees of freedom imposed by confinement. Together with the particle migration towards the walls, this leads to the formation of ordered wall layers, leaving behind lower volume fraction, disordered middle layers. Particle migration appears to be a general characteristic of the approach towards the phase boundary; moving towards this boundary, either by adjusting the volume fraction or the shear rate, results in the appearance of a range of layer volume fractions preceding any phase separation. In contrast, Cohen et. al.<sup>12</sup> found that systems in contact with a reservoir do not exhibit such behavior. Instead, the balance between viscous stress and osmotic pressure sets a high volume fraction throughout the system leading to the formation of dense, ordered particle structures.

The onset of particle migration is accompanied by a noticeable rise in the colloidal granular temperature. Consider, for example, the highest volume fraction systems. These all consist of four ordered layers in steady state for the shear rates we have investigated. Moving from lower to higher shear rate systems, we observe a fairly steady rise in the kinetic energy per unit mass for the fluid. However, the colloidal granular temperatures remain approximately constant among the lower shear rate systems, only increasing at the onset of particle exchange among layers (see Fig. 5C). Once the phase boundary is crossed, and disordered layers begin to form, we observe an increase in both the colloidal granular temperature and the kinetic energy in the fluid, particularly in the disordered layers (see Figs. 5A and B). The velocity deviations in the fluid are illustrated in Fig. 6 for one such system. Here we have subtracted off the average velocity profile in the system. Clearly, the velocity field can be quite complicated, particularly in the disordered middle layers, where the chaotic motion of the colloidal particles can lead to disordered fluid flow around them.

To gain a better understanding of the mechanisms driving the order-disorder (and vice-versa) transitions in the layers, we monitor the evolution of the systems as a function of time. Figure 7 shows the results for three different simulations, which we will refer to as systems A, B and C. Compar-



**Fig. 4** Phase diagram illustrating the per layer system behavior as a function of volume fraction and shear rate in each layer. Markers corresponding to a blue symbol on a white circular background are associated with hexagonally ordered layers, while those with a white symbol on a red background denote disordered layers. At a given shear rate, markers with the same central symbol correspond to layers from the same physical system. For example, at a shear rate of  $1.7\mu s^{-1}$  there are four markers each with a central diamond symbol. These correspond to layers from a system with total volume fraction 0.521 which has phase separated into 1 disordered and 3 ordered layers. Similarly, squares, 5 point stars and rectangles are also associated with systems with a total volume fractions of 0.521, clubs, downward pointing triangles, and circles correspond to a total volume fraction of 0.588, and upward pointing triangles, clovers, and 6 point stars correspond to a total volume fraction of 0.645. For purposes of comparison the location of the ordered, disordered, and coexistence region for a colloidal system in the absence of shear is indicated on the left.

ing our order parameter to the experimental results of Wu et al.<sup>17</sup>, we find a qualitatively similar behavior. We observe the same initial rapid decrease in order followed by fluctuating values. For system B, in which the two inner layers are disordered, the variations in order are somewhat large, ranging from  $\sim 0.4-0.6$ . As discussed by Wu et al., these fluctuations suggest the formation of local ordered domains which regularly appear and subsequently re-melt. This behavior is confirmed in our simulation. However, the magnitude of our fluctuations are smaller than those observed by Wu et al. and are further reduced in our lower volume fraction systems. These fluctuations in layer order are clearly related to the fluctuations exhibited by the layer particle number, with increased particle numbers resulting in higher levels of order. In addition, particle exchange between layers appears to directly affect the level of order in the systems. The initial drop in order ( $\langle |\psi_6| \rangle$  decreasing to values below 0.6), as exhibited by systems A and

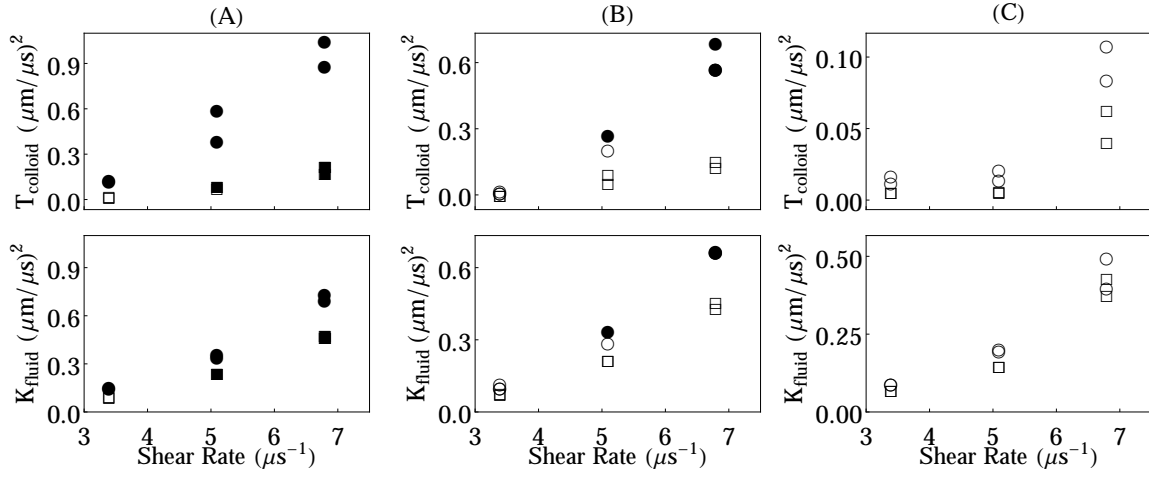


**Fig. 5** Per layer, steady-state granular temperature for the colloids (top panel) and kinetic energy per unit mass for the fluid (lower panel). (A) Volume fraction of 0.521, (B) 0.588, and (C) 0.645. Squares: wall layers. Circles: middle layers. Open symbols correspond to ordered and closed to disordered layers. Note the use of different vertical axes for each plot.

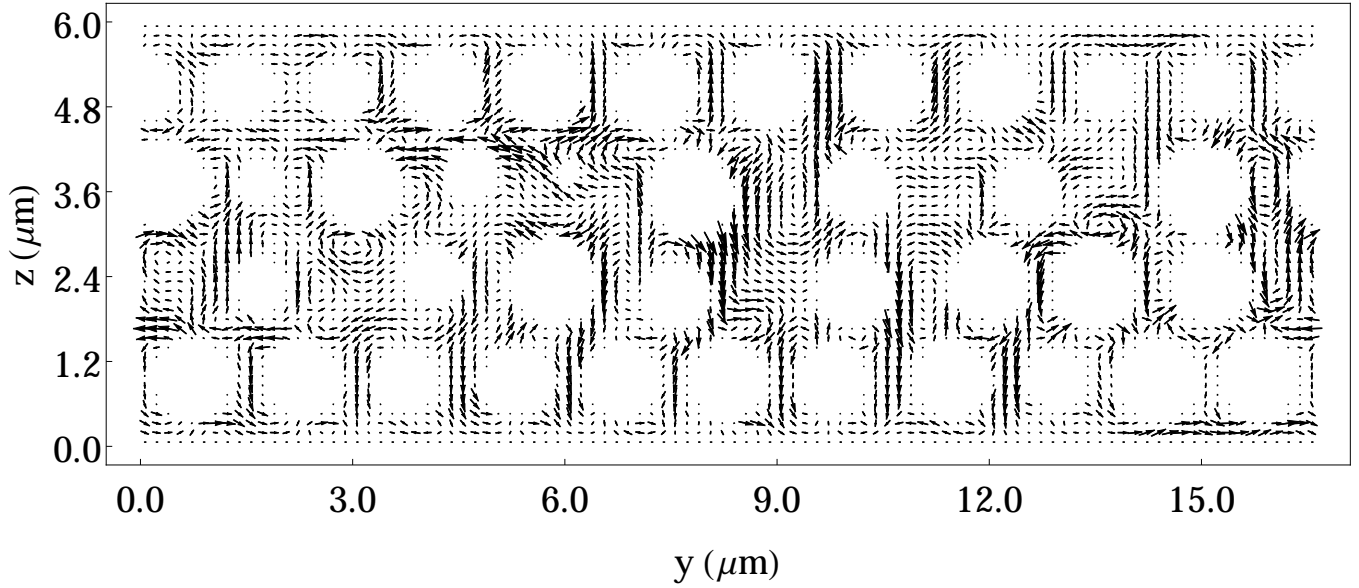


**Fig. 6** Fluid velocity deviations in the  $yz$ -plane, calculated by subtracting off the average fluid velocity at each  $z$  position, for a system with volume fraction = 0.588, and shear rate =  $6.8 \mu\text{s}^{-1}$ . Here, the colloidal particles are moving and rotating with the fluid, and the fluid inside them has been removed for illustrative purposes.

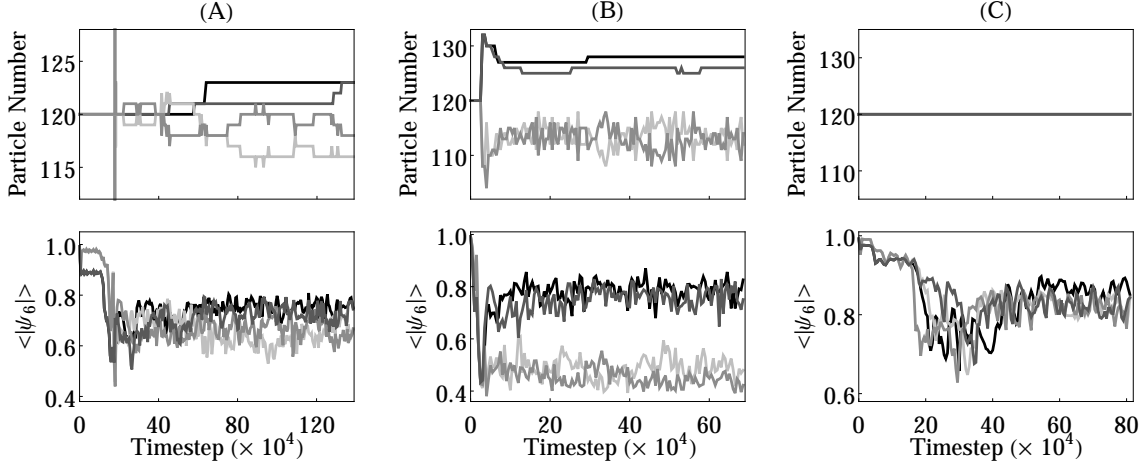


**Fig. 7** Particle number and order parameter amplitude,  $\langle |\psi_6| \rangle$ , as a function of time for each layer. (A) volume fraction = 0.588, shear rate =  $3.4 \mu s^{-1}$ , (B) volume fraction = 0.588, shear rate =  $6.8 \mu s^{-1}$ , (C) volume fraction = 0.645, shear rate =  $3.4 \mu s^{-1}$ . Darker grey: particle layers near the walls. Lighter grey: middle layers.

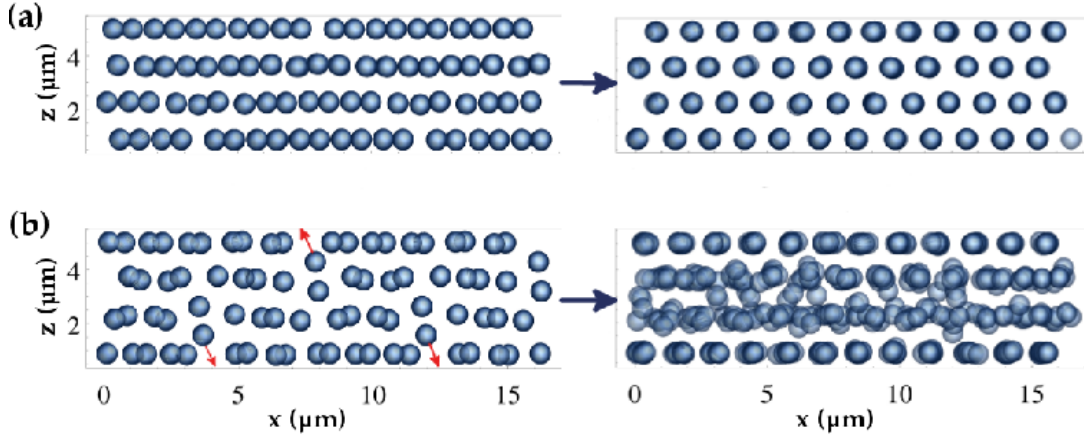


**Fig. 8** Snapshots of configurations in the  $x$ - $z$  plane, for (a) volume fraction = 0.645, shear rate =  $3.4 \mu s^{-1}$ , and (b) volume fraction = 0.588, shear rate =  $6.8 \mu s^{-1}$ . Left: early times in the simulation. Right: the steady-state configurations. Note that the size of the colloidal particles has been reduced here for clarity.



B directly corresponds to the emergence of particle exchange. For system C, in which no such exchange occurs,  $\langle |\psi_6| \rangle$  never falls below 0.65. The initial particle exchange appears to proceed as follows: As previously mentioned, shear along the  $y$ -direction is unfavourable to the initial particle configuration, requiring particles in adjacent layers to “hop” over one another. This leads to particle motion in the  $z$ -direction, which causes particles to push on adjacent layers leading to the formation of voids. We find this behavior to be exhibited by all of the systems, even those which do not experience particle exchange (see, e.g., the left panel of Fig. 8a, corresponding to the early time behavior of system C). However, for systems in which the particle size is small enough, and the  $z$ -motion large enough, particles from neighbouring layers are able to move into the voids and exchange occurs. This is illustrated in the left hand panel of Fig. 8b, showing the early time behavior of system B.

While systems A and C both reach steady-state configurations consisting of four ordered layers, the fact that particle exchange occurs for one system and not the other clearly points to different mechanisms responsible for the layer reordering. Particle exchange tends to induce disorder, effectively melting the layers, which subsequently reorder. In contrast, in the absence of particle exchange, regions within the layer undergo a reordering. In both cases, the result is the formation of hexagonal particle layers aligned along the flow (right hand panel of Fig. 8a).

When particle exchange does occur among layers, aside from the initial drop in order that accompanies the onset of exchange, the degree of layer order throughout the simulation is directly related to the quantity and frequency of exchange. For example, even though all four layers in system A reorder, a moderate amount of particle exchange occurs for the middle layers. Correspondingly,  $\langle |\psi_6| \rangle$  is reduced to the range  $0.6 \leq \langle |\psi_6| \rangle \leq 0.7$  compared with the outer layers, which experience almost no exchange and have higher values for  $\langle |\psi_6| \rangle$ . Even more frequent particle exchange is associated with even lower values for the  $\langle |\psi_6| \rangle$ . For system B, in which the inner layers experience a substantial and sustained particle exchange, the order parameter amplitude falls to  $0.4 \leq \langle |\psi_6| \rangle \leq 0.55$ , corresponding to disordered layers. This particle exchange, illustrated in the right hand panel of Figure 8b, persists along with the disorder in the simulations, and is associated with both increased colloidal granular temperature and kinetic energy in the fluid.

## 4 Conclusions

In this work, we investigated the effects of volume fraction and shear rate on the behavior of confined colloidal particles. Starting from an initially ordered arrangement, the resulting steady-state configurations consist of particles which either re-

order into hexagonally ordered layers aligned along the flow, form purely disordered layers, or phase separate into higher volume fraction ordered layers near the walls, and lower volume fraction disordered middle layers. By plotting the per layer behavior as a phase diagram, we illustrate the effects of the volume fraction and shear stress in our systems on the colloidal order-disorder transition. An examination of the layer particle number as a function of time reveals that the onset of disorder in the systems is characterized by the emergence of particle exchange among layers: Systems which do not experience exchange never pass through the disordered phase. When particle exchange occurs, there is a direct relation between the amount of exchange, and a reduction in the layer order, with disordered layers experiencing substantial and sustained particle exchange. It is important to note that all of these effects are driven by the hydrodynamic flow rather than thermal noise. At times, the resulting particle motion can be random, disordered and lacking any periodicity, which naturally leads to disordered fluid flow around the particles despite the overall average imposed shear gradient.

## Acknowledgments

We thank the Natural Science and Engineering Research Council of Canada (NSERC) for financial support. This research has been enabled by the use of computing resources provided by WestGrid, ShareNet and Compute/Calcul Canada.

## References

- 1 B. J. Ackerson, and N. A. Clark, Phys. Rev. Lett. **46** 123 (1981).
- 2 M. J. Stevens, M. O. Robbins, and J. F. Belak, Phys. Rev. Lett. **66** 3004 (1991).
- 3 D. Derks, Y. Wu, A. van Blaaderen, and A. Imhof, Soft Matter **5** 1060 (2009).
- 4 B. J. Ackerson and N. A. Clark, Phys. Rev. A **30** 906 (1984).
- 5 C. Dux, H. Versmold, V. Reus, T. Zemb, and P. Lindner, J. Chem. Phys. **104** 6369 (1996).
- 6 M. D. Haw, W. C. K. Poon, and P. N. Pusey, Phys. Rev. E **57** 6859 (1998).
- 7 K. Yeo and M. R. Maxey, Phys. Rev. E **81** 051502 (2010).
- 8 S. R. Rastogi, N. J. Wagner and S. R. Lustig, J. Chem. Phys. **104** 9234 (1996).
- 9 R. M. Amos, J. G. Rarity, P. R. Tapster, T. J. Shepherd, and S. C. Kitson, Phys. Rev. E **61** 2929 (2000).
- 10 T. Kanai, T. Sawada, A. Toyotama, and K. Kitamura, Adv. Funct. Mater. **15** 25 (2005).

- 11 J. J. Cerdà, T. Sintes, C. Holm, C. M. Sorensen, and A. Chakrabarti, *Phys. Rev. E* **78** 031403 (2008).
- 12 I. Cohen, T. G. Mason and D. A. Weitz, *Phys. Rev. Lett.* **93** 046001 (2004).
- 13 A. Reinmüller, E. C. Oğuz, R. Messina, H. Löwen, H. J. Schoöpe and T. Palberg, *Eur. Phys. J. Special Topics* **222** 3011 (2013).
- 14 R. Besseling, E. R. Weeks, A. B. Schofield, and W. C. K. Poon, *Phys. Rev. Lett.* **99** 028301 (2007).
- 15 N. Koumakis, A. Pamvouxoglou, A. S. Poulos, and G. Pektikidis, *Soft Matter* **8** 4271 (2012).
- 16 C. Eisenmann, C. Kim, J. Mattsson and D. A. Weitz, *Phys. Rev. Lett.* **104** 035502 (2010).
- 17 Y. L. Wu, D. Derks, A. van Blaaderen and A. Imhof, *Proc. Natl. Acad. Sci. USA* **106** 10564 (2009).
- 18 M. Das, S. Ramaswamy and G. Ananthakrishna, *Europhys. Lett.* **60** 636 (2002).
- 19 T. Palberg and R. Biehl, *Faraday Discuss.* **123** 133 (2003).
- 20 X. Cheng, X. Xu, S. A. Rice, A. R. Dinner and I. Cohen, *Proc. Natl. Acad. Sci. USA* **109** 63 (2012).
- 21 N. Y. C. Lin, X. Cheng, and I. Cohen, *Soft Matter* **10** 1969 (2014).
- 22 R. Messina and H. Löwen, *Phys. Rev. E* **73** 011405 (2006).
- 23 S. Butler and P. Harrowell, *Phys. Rev. E* **52** 6424 (1995).
- 24 S. Plimpton, *J. Comp. Phys.* **117** 1 (1995).
- 25 F. E. Mackay, S. T. T. Ollila and C. Denniston, *Comput. Phys. Comm.* **184** 2021 (2013).
- 26 F. E. Mackay, C. Denniston, *J. Comput. Phys.* **237** 289 (2013).
- 27 A. Baldassarri, A. Barrat, G. D’Anna, V. Loreto, P. Mayor and A. Puglisi, *J. Phys.: Condens. Matter* **17** S2405 (2005).
- 28 R. Biehl and T. Palberg, *Europhys. Lett.* **66** 291 (2004).